

Unusual magnetic and structural transformations of DyFe₄Ge₂

J. Liu,^{1,2,*} D. Paudyal,¹ Y. Mudryk,¹ J. D. Zou,¹ K. A. Gschneidner, Jr.,^{1,2} and V. K. Pecharsky^{1,2}

¹The Ames Laboratory, U.S. Department of Energy, Iowa State University, Ames, Iowa 50011-3020, USA

²Department of Materials Science and Engineering, Iowa State University, Ames, Iowa 50011-2300, USA

(Received 3 May 2013; revised manuscript received 27 June 2013; published 19 July 2013)

Magnetization of DyFe₄Ge₂ measured as function of temperature in a 1 kOe magnetic field indicates antiferromagnetic (AFM) ordering at $T_N = 62$ K followed by two spin reorientation transitions at $T_{f1} = 52$ and $T_{f2} = 32$ K and one unusual anomaly at 15 K (T_{f3}). Three transitions (T_{f1} , T_{f2} , and T_N) are further confirmed by heat capacity measurement in a zero magnetic field. The two low-temperature magnetic transitions are broadened and gradually vanish when the applied magnetic field exceeds 30 kOe, and the AFM transition shifts toward low temperatures with an increasing magnetic field. The reentrant magnetic glassy state is observed below the freezing point of $T_{f3} = 15$ K. Two field-induced metamagnetic phase transitions are observed between 2 and 50 K in fields below 140 kOe. A temperature-magnetic-field phase diagram has been constructed. The first-principles electronic structure calculations show that the paramagnetic tetragonal structure of DyFe₄Ge₂ is stable at high temperatures. The calculations with collinear Dy spins confirm ferrimagnetic orthorhombic DyFe₄Ge₂ as the ground-state structure.

DOI: [10.1103/PhysRevB.88.014423](https://doi.org/10.1103/PhysRevB.88.014423)

PACS number(s): 61.50.Ks, 75.30.-m, 71.20.Eh, 71.15.Mb

I. INTRODUCTION

Rare-earth-based intermetallic compounds continue to draw considerable attention due to their importance in understanding of fundamental structure-property relationships and the potential for practical applications based on a variety of phenomena, including strong magnetocaloric, magnetoelastic, magnetoresistance, and other effects.¹⁻³ Among numerous extended families of intermetallics, the so-called R_5T_4 compounds formed by the rare-earth and nonmagnetic group 14 elements (that may be partially substituted by group 13 or 15 elements) have attracted considerable attention after the discovery of the giant magnetocaloric effect (GMCE) in the Gd₅Si_xGe_{4-x} system.⁴⁻⁸ At present, it is well known that the giant magnetocaloric effect is always associated with either a coupled magnetostructural transformation⁹⁻¹³ or an itinerant electron metamagnetism (IEM).¹⁴ Since there are only a few IEM compounds which exhibit a GMCE, we believe it is more fruitful to investigate other compounds that may exhibit magnetostructural transformations.

Ternary intermetallics RFe_4Ge_2 ($R = Y, Dy, Er, Ho, Tm,$ and Lu) are attractive due to their peculiar magnetic properties and, particularly, because of reportedly strong magnetoelastic transitions.¹⁵⁻¹⁹ Their peculiarity originates from two factors: one is the presence of both R and Fe magnetic atoms with different anisotropies leading to three competing (R - R , Fe-Fe, and R -Fe) ordering mechanisms, and the other is the geometrical frustration associated with the Fe atomic arrangement.¹⁸ It was found that the compounds RFe_4Ge_2 ,¹⁷ where $R = Y, Dy, Ho, Er,$ and Lu , crystallize with the tetragonal ZrFe₄Si₂-type structure (space group $P4_2/mnm$) at room temperature. The crystal structure of the DyFe₄Ge₂ compound is illustrated in Fig. 1 with its unit-cell shown by using solid lines. It consists of infinite double columns of trigonal prisms, and it may also be viewed as a body-centered array of Dy atoms, each atom being surrounded by six Ge atoms arranged into a distorted octahedron. The Fe atoms are located around the 4₂ axes of the crystal lattice of the unit cell. Each Ge atom is surrounded by a trigonal prism of two R and four Fe atoms

augmented by three additional ones (two Fe atoms and one R atom) opposite the rectangular faces of the prism. It was also reported that, at low temperatures, below 55 K, the DyFe₄Ge₂ compound adopts the orthorhombic (space group $Cmmm$) structure.^{18,20} The unit-cell of the orthorhombic structure is shown with the dashed line in Fig. 1. The unit-cell volume of the low-temperature orthorhombic phase is twice that of the high-temperature tetragonal phase.

The RFe_4Ge_2 compounds originally have been reported to order ferromagnetically with T_C varying from 643 K for $R = Lu$ to 963 K for $R = Y$.^{21,22} However, based on the low-temperature neutron diffraction investigations and x-ray diffraction (XRD) studies of the compounds DyFe₄Ge₂, ErFe₄Ge₂, and HoFe₄Ge₂,^{15,17,18,20,23,24} the ferromagnetic nature at such high temperatures was not confirmed. Moreover, the ⁵⁷Fe Mössbauer spectroscopy and magnetization measurements in high magnetic fields^{22,25,26} did not reveal any ferromagnetic ordering at room temperature in these RFe_4Ge_2 intermetallics. The neutron diffraction measurements show that the simultaneous structural and magnetic transitions of DyFe₄Ge₂ occurs at 55 K and the subsequent magnetic transitions in the magnetically ordered state are at $T_{f1} = 45$ and $T_{f2} = 28$ K.^{18,20}

Although the magnetic structure of DyFe₄Ge₂ has been reported,^{18,20} the detailed magnetic behaviors as functions of temperature and applied field are lacking. Therefore, we have performed a systematic investigation of the magnetic and thermal properties of DyFe₄Ge₂ in order to reveal the underlying mechanism of these magnetic phase transitions. We explore the influence of the temperature and applied field on their phase transitions by using dc and ac magnetic measurements, the thermal properties by heat capacity measurement, and the structural transition by temperature-dependent x-ray diffraction. Finally, the H - T magnetic phase diagram of DyFe₄Ge₂ is constructed taking into account both the temperature and the magnetic field induced magnetic transitions. Electronic structure calculations have also been performed to confirm the stable magnetic states in both the low- and the high-temperature crystal structures of DyFe₄Ge₂.

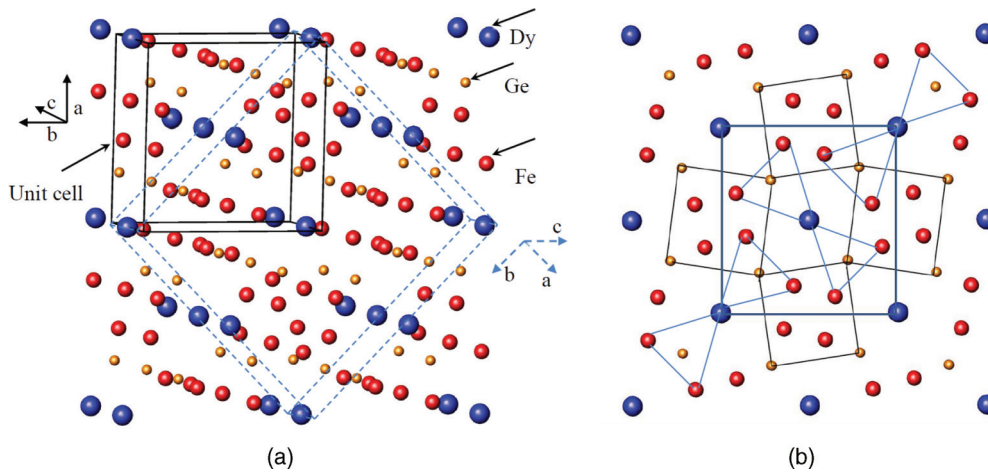


FIG. 1. (Color online) (a) Crystal structure of the tetragonal DyFe_4Ge_2 at room temperature (the unit-cell is shown using solid lines). The dashed lines delineate the unit-cell of the orthorhombic low-temperature structure of DyFe_4Ge_2 . (b) Projection onto the (001) plane of the tetragonal DyFe_4Ge_2 .

II. EXPERIMENTAL DETAILS

The alloy with the DyFe_4Ge_2 composition was prepared by arc melting the pure elements (purity: Dy: 99.98 wt % with respect to all other elements in the periodic system, Fe: 99.9838 wt % and Ge 99.999+ wt %) on a water-cooled copper hearth under an argon atmosphere. The alloys were flipped and were remelted four times to ensure compositional homogeneity. The room-temperature crystal structure of the sample was investigated by x-ray powder diffraction using $\text{Cu } K\alpha_1$ radiation, and the diffraction pattern confirms that the specimen crystallizes in the ZrFe_4Si_2 -type structure.

The ac magnetic susceptibility and dc magnetization as functions of temperature were measured by using a superconducting quantum interference device (SQUID) magnetometer MPMS XL-7 and a vibrating sample magnetometer of the physical property measurement system (PPMS) from Quantum Design, Inc. The temperature dependence of the magnetization was measured in the range from 2 to 300 K in magnetic fields from 1 to 70 kOe by using the SQUID. The temperature-dependent magnetization data were collected in various applied magnetic fields under zero-field-cooled-warming (ZFC), field-cooled-cooling (FCC), and field-cooled-warming (FCW) protocols. The magnetization isotherms, between 2 and 80 K, were measured in magnetic fields up to 140 kOe in the PPMS. Each isothermal plot was obtained by measuring the DyFe_4Ge_2 sample in the virgin state after zero-field cooling from the paramagnetic (PM) state. The ac magnetic susceptibility was measured using the SQUID magnetometer with an ac drive magnetic field of 5 Oe and frequencies of 1, 10, 100, and 1000 Hz. The heat capacity was measured using a homemade adiabatic heat-pulse calorimeter.²⁷ Measurements were performed in the temperature range from about 2 to 350 K in applied magnetic fields from 0 up to 50 kOe. Temperature dependent x-ray powder diffraction data were collected on a Rigaku TTRAX powder diffractometer using $\text{Mo } K\alpha$ radiation in the 2θ range of 7° to 55° from 5 to 300 K.

III. RESULTS AND DISCUSSION

A. Room-temperature x-ray diffraction and energy dispersive x-ray spectroscopy

The crystal structure of the investigated alloy was determined by the XRD, and both the lattice parameters and the atomic positions were refined by using the Reitveld refinement program LHPM-RIETICA.²⁸ The refined room-temperature XRD pattern of DyFe_4Ge_2 is shown in Fig. 2. The alloy contains small amounts of minor impurity phases DyFe_2Ge_2 (~ 4 wt %) and Fe (~ 2 wt %). Our data confirm that DyFe_4Ge_2 crystallizes in the ZrFe_4Si_2 -type structure with the following

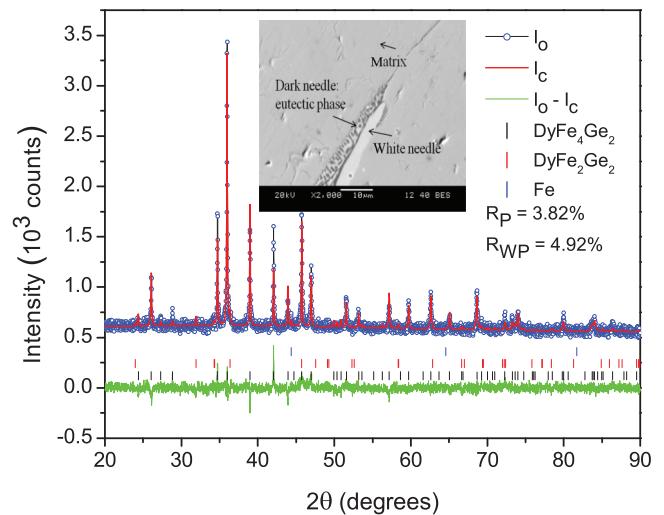


FIG. 2. (Color online) The Rietveld refined room-temperature x-ray diffraction pattern of DyFe_4Ge_2 . The open circles represent experimental data points, whereas, the lines represent the calculated pattern. The difference $I_{\text{obs}} - I_{\text{calc}}$ is shown at the bottom of the plot. Vertical bars under the patterns indicate the calculated positions of Bragg peaks of the main phase DyFe_4Ge_2 and minor phases Fe and DyFe_2Ge_2 . The inset is a backscattered electron image of the DyFe_4Ge_2 specimen after polishing.

lattice parameters: $a = 7.3027(9)$ and $c = 3.8660(5)$ Å. The Dy atoms occupy $2b$ sites $(0,0,0.5)$, Fe atoms occupy $8i$ sites $(x,y,0)$ with $x = 0.1483(10)$ and $y = 0.4099(9)$, and Ge atoms occupy $4g$ sites $(x,-x,0)$ with $x = 0.2837(8)$. Qualitative composition analyses of the polished samples were performed by energy-dispersive x-ray spectroscopy using a JEOL 5910LV scanning electron microscope. The backscattered electron image of DyFe_4Ge_2 is shown in the inset of Fig. 2. The gray matrix has a composition of Dy:Fe:Ge = 1:4:2; the dark needle-shaped eutectic phase is $\text{Fe}_{1-x}\text{Ge}_x$, and the white phase is DyFe_2Ge_2 .

B. Magnetic properties

Figure 3 shows the temperature dependencies of magnetization of DyFe_4Ge_2 measured in an applied field of 1 kOe under ZFC, FCC, and FCW conditions. Multiple magnetic transitions are clearly observed. An antiferromagnetic (AFM) like transition occurs at $T_N = 62$ K. Additional magnetic transitions are observed at 52 K (T_{f1}) and 32 K (T_{f2}). There is also another anomaly that occurs at about 15 K, which can only be observed in the low-field ZFC data; this anomaly, marked as T_{f3} , was not reported in the past. We note that DyFe_2Ge_2 orders antiferromagnetically with a Néel temperature of 3.35 K (Ref. 29) and, therefore, is not expected to play any role in the magnetic anomalies observed at 15 K and above. Furthermore, our magnetization data of Fig. 3 do not show any anomalies in the vicinity of this transition point, thereby, indicating that the impurity has no measureable effect on the magnetic behavior of the main phase even near the magnetic ordering temperature of the impurity.

Multiple magnetic transitions are not unique and are often observed in rare-earth intermetallics because they can arise from the competition and interplay of the Ruderman-Kittel-Kasuya-Yosida (RKKY) indirect exchange interactions, quadrupolar, magnetostrictive, and magnetoelastic interac-

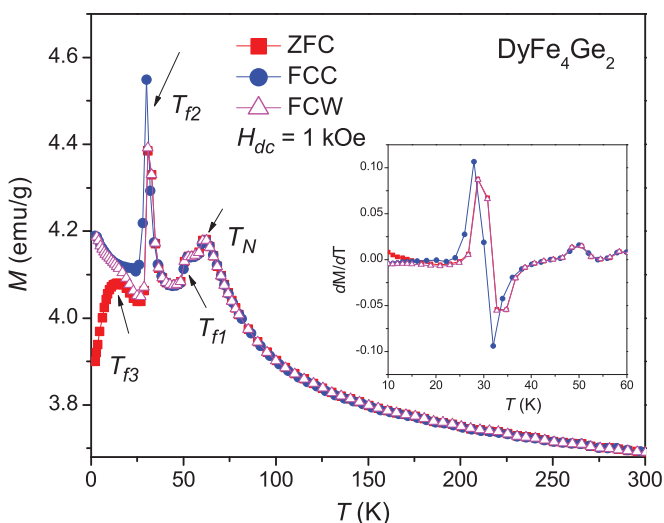


FIG. 3. (Color online) Temperature dependencies of the magnetization of DyFe_4Ge_2 measured in a 1 kOe applied magnetic field upon ZFC, FCC, and FCW. The inset is the temperature dependence of the first derivative of the magnetization with respect to temperature (dM/dT) under ZFC, FCC, and FCW conditions.

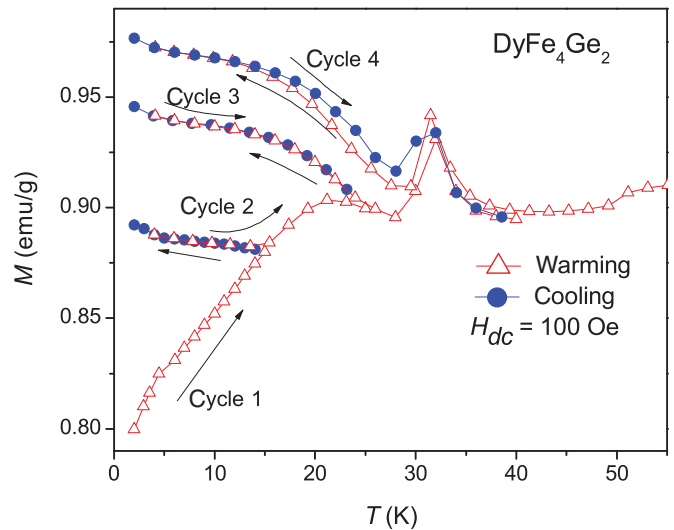


FIG. 4. (Color online) Path dependence of the magnetization (M) of zero-field-cooled DyFe_4Ge_2 .

tions. In DyFe_4Ge_2 , multiple spin reorientations are, indeed, expected because the two magnetic elements with three competing (R - R , Fe-Fe, and R -Fe) interactions are present.

Besides the multiple magnetic transitions discussed above, obvious thermomagnetic irreversibility among the ZFC, FCC, and FCW $M(T)$ curves is present as is also seen in Fig. 3. From the derivative of the $M(T)$ data shown in the inset of Fig. 3, the T_{f2} , on heating and cooling (defined as the temperature at which dM/dT changes sign), is 32 and 30 K, respectively. The irreversibility between the ZFC and the FCC is commonly observed in magnetic compounds with narrow domain wall pinning effects, e.g., ferromagnets with magnetocrystalline anisotropy, spin glasses, and systems with competing ferromagnetic and antiferromagnetic interactions.³⁰⁻³⁴ Intrinsic geometrical frustrations of a complex spin system may also contribute to the irreversibility between ZFC and FCC curves.

In addition to the irreversibility between the ZFC and the FCC data, FCC and FCW data also exhibit a small but measurable irreversibility as shown in Fig. 3. The irreversibility between the FCC and the FCW curves strongly suggests a first-order nature of phase transition at T_{f2} . The first-order nature of this transition was also identified from thermal hysteresis observed in the behavior of lattice parameters measured by XRD and neutron diffraction measurements.^{18,20} It is also interesting to note that M_{FCW} is lower than M_{FCC} between 12 and 32 K. The occurrence of inverse hysteresis ($M_{\text{FCW}} \leq M_{\text{FCC}}$) requires additional low-field magnetization measurements to find out whether the magnetization below 32 K belongs to an equilibrium state or not. Therefore, several thermal cycling magnetization experiments were undertaken as shown in Fig. 4. The sample was initially cooled to 2 K without a field and then was heated from 2 to 15 K in a 100 Oe magnetic field. Subsequently, the sample was cooled from 15 K back to 2 K and then from 2 to 25 K, from 25 to 2 K, from 2 to 40 K, from 40 to 2 K, and finally, from 2 to 55 K. The results clearly show that magnetization at 2 K increases after the first (2–15–2 K) temperature cycle; it keeps increasing in the subsequent cycles. As is known, geometrical frustration

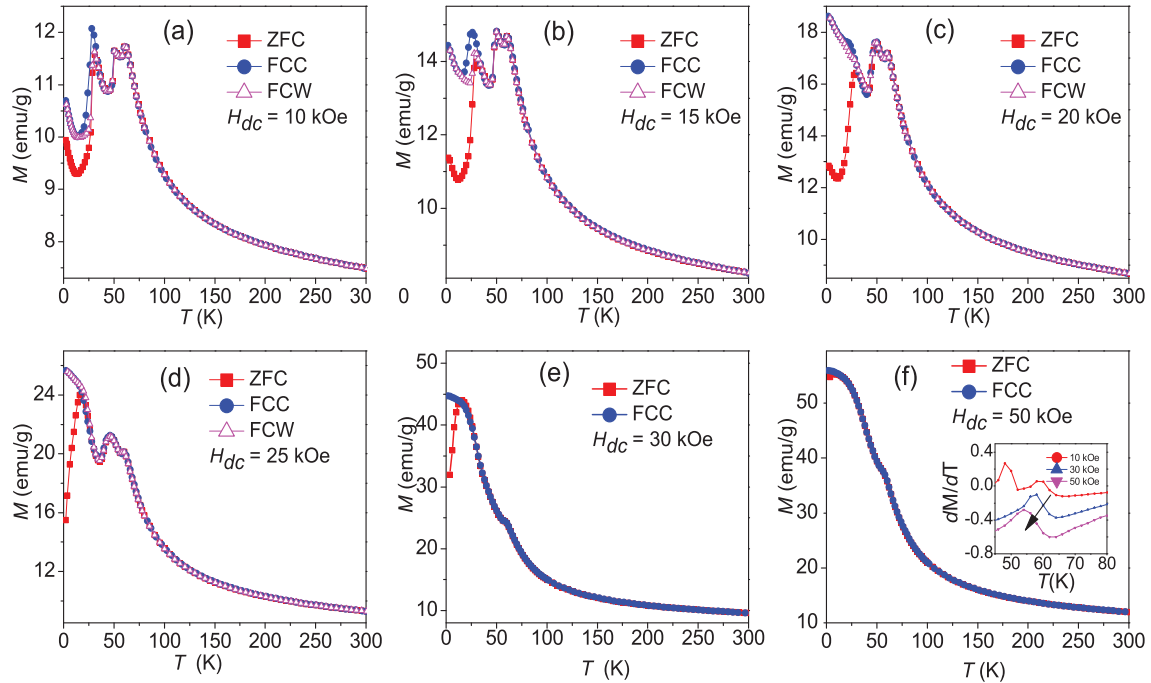


FIG. 5. (Color online) Temperature dependencies of the magnetization of DyFe_4Ge_2 measured in 10, 15, 20, and 25 kOe applied magnetic fields upon ZFC, FCC, and FCW conditions and the 30 and 50 kOe applied magnetic field upon ZFC and FCC conditions. The inset of panel (f) shows the temperature dependence of the first derivative of the magnetization with respect to temperature (dM/dT) in ZFC conditions in 10, 30, and 50 kOe.

affects the stability of antiferromagnetic structures.^{35,36} In addition, the low-temperature XRD analysis showed that a compact Fe tetrahedral configuration with antiferromagnetic Fe-Fe interactions is prone to the geometrical frustration.¹⁸ Therefore, the data of Fig. 4 show that the magnetization depends upon the thermal history of the ordered state, establish the metastable nature of the low- T antiferromagnetic state, and suggest probable intrinsic geometrical frustration below 32 K.

Figure 5 shows the ZFC, FCC, and FCW $M(T)$ plots for DyFe_4Ge_2 measured in applied fields of 10, 15, 20, and 25 kOe and ZFC and FCC curves in 30 and 50 kOe. We note that a broad peak observed at $T_{f3} = 15$ K in Fig. 3 disappears in fields 10 kOe and higher, but a minimum in the magnetization, related to the T_{f3} transition, is still observed at this temperature at fields lower than 20 kOe. The $M(T)$ curves measured in magnetic fields from 10 to 50 kOe (Fig. 5) clearly show that below 30 kOe, the low-temperature transitions are complex. The temperature of the transition at T_{f2} decreases from 32 K in a 1 kOe applied field to 30 K in 15 kOe, to 28 K in 20 kOe, and to 18 K in 25 kOe. The same trend is observed for the T_{f1} transition: it is decreased from 52 to 50 K at 10 and 20 kOe. At 25 kOe, it moves to 46 K and then disappears when the field exceeds 30 kOe. It is also interesting to note that between 1 and 20 kOe, as the applied field increases, the anomaly at T_{f2} (32 K) becomes weaker, whereas, the anomaly related to T_{f1} becomes stronger. At 1 kOe, the transition at T_{f1} is only manifested as a shoulder (Fig. 3), however, at 20 kOe, it becomes a relatively sharp peak.

As shown in the inset of panel (f) in Fig. 5, T_N shifts to lower temperatures as the applied field increases: from 62 K at 1 kOe to 56 K at 50 kOe, which, again, indicates that the AFM interactions are dominant in the low-temperature

range.³⁷ In addition, the ZFC magnetization is always smaller than the FCC one at low temperatures. We also note that the bifurcation between ZFC and FCC curves exists even at 50 kOe, shifting to lower temperatures as the applied field increases. This also suggests that the magnetically ordered state is a complex magnetic structure with predominant antiferromagnetic interactions.

These results agree with neutron diffraction data on DyFe_4Ge_2 . Three different magnetic structures of DyFe_4Ge_2 have been proposed below T_N .²⁰ At temperatures below T_{f2} , the Fe and Dy sublattices are three-dimensional canted antiferromagnets. Between T_{f1} and T_N , the Dy moments are collinearly aligned, and Fe moments are planar arranged in the (001) plane. In the temperature range between T_{f1} and T_{f2} the magnetic structure is incommensurate.

The ac magnetic susceptibility has been measured as a function of temperature in a zero dc magnetic field, and its real component is shown in Fig. 6. The real component of the ac susceptibility χ' shows a sharp peak at about 32 K (T_{f2}), a steplike anomaly at 51 K close to T_{f1} [inset (a)], and a slope change around 62 K (T_N), which are consistent with temperatures determined from the dc magnetization data. The magnetic anomaly at 15 K under the 1 kOe applied field $M(T)$ curve is not observed in the $\chi'(T)$ data. In addition, weak but measurable frequency dependence is observed in the χ' data below T_{f2} . The susceptibility above T_N does not decrease with temperature as expected for a paramagnet due to a small amount of ferromagnetic impurity phase $\text{Fe}_{1-x}\text{Ge}_x$; here, the 5 Oe driving field is not strong enough to saturate the impurity. When biased by a 1 kOe dc magnetic field, the ac magnetic susceptibility shows paramagnetic behavior above T_N as displayed in inset (b) of Fig. 6.

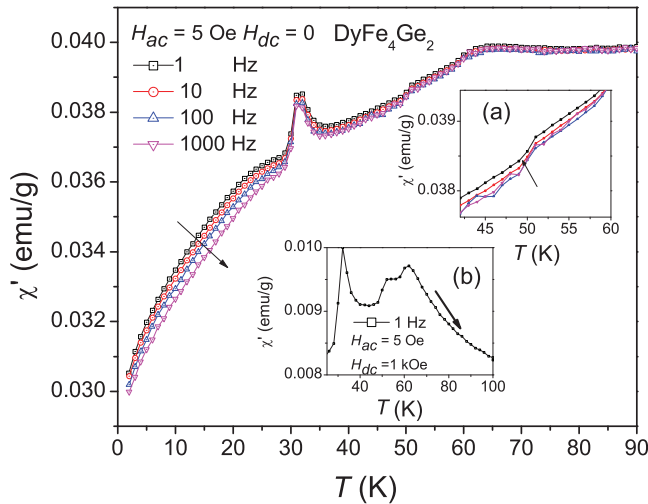


FIG. 6. (Color online) Temperature dependencies of the real component of ac susceptibility (χ') of DyFe_4Ge_2 collected in a 5 Oe ac field, zero dc field, and frequencies from 1 to 1000 Hz. Inset (a) is the expanded view of the details of the region around the T_{f1} transition. Inset (b) is the ac susceptibility curve measured in the presence of the 1 kOe bias dc magnetic field.

Figure 7 shows the magnetization isotherms of DyFe_4Ge_2 measured at 2, 5, 10, and 20 K. A weak ferromagnetic signa-

ture, seen in all $M(H)$ data, reflects the presence of a minor ferromagnetic impurity $\text{Fe}_{1-x}\text{Ge}_x$. The magnetization at 2 K increases slowly below 20 kOe, suggesting an antiferromagnetic ground state. With a further increase in the field, when the first critical field (H_{c1}) is reached, the magnetization exhibits a metamagnetic transition. Following the first relatively sharp steplike transition, there is a second and broader field-induced metamagnetic transition (H_{c2}) above 60 kOe. It is worth noting that both transitions show hysteresis, confirming their first-order nature. In addition, during the second increase in the magnetic field, the magnetization curve does not follow the virgin magnetization path at 2 K. It reaches the first step and first saturation faster than the virgin magnetization curve, but the demagnetization path is the same in these two processes. At 20 K, the second magnetization curve (including the demagnetization curve) as shown in Fig. 7 becomes identical to the virgin field-increasing and decreasing measurement.

Thus, the field-induced metamagnetic transition in DyFe_4Ge_2 is fully reversible above 20 K. A similar change in the envelope $M-H$ curves at different temperatures was observed in Gd_5Ge_4 , and a freezing/unfreezing transition into a magnetic glasslike state was suggested to explain this behavior.³⁸⁻⁴¹ Considering the metastabilities observed in the low-temperature state of DyFe_4Ge_2 (Fig. 4) and the isothermal magnetization results, the T_{f3} transition at 15 K may be a freezing point. Below this temperature, the

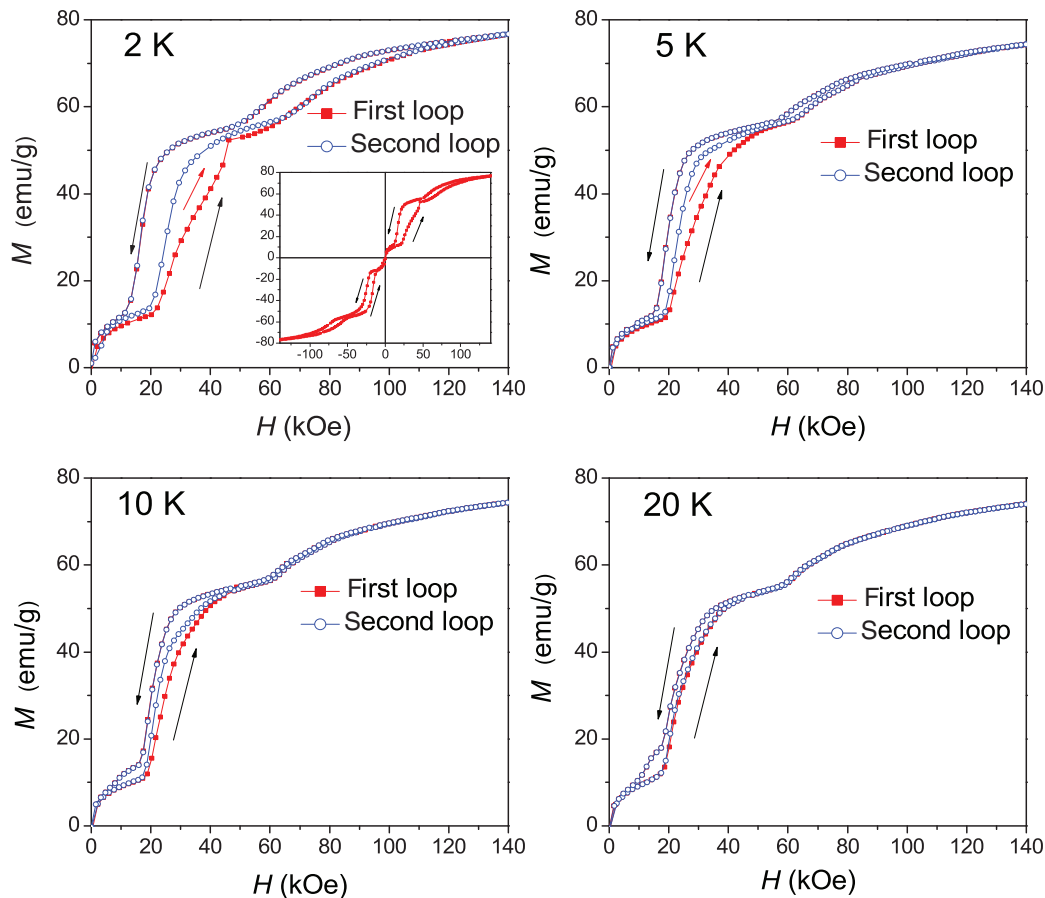


FIG. 7. (Color online) Magnetization isotherms of DyFe_4Ge_2 measured in applied magnetic fields from 0 to 140 kOe at 2, 5, 10, and 20 K. A weak ferromagnetic signature seen below 10 kOe is due to the presence of about 2 wt % of $\text{Fe}_{1-x}\text{Ge}_x$.

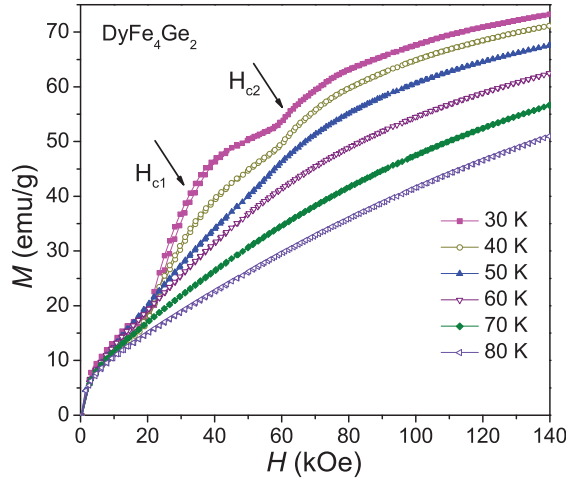


FIG. 8. (Color online) Magnetization isotherms of DyFe_4Ge_2 measured in applied magnetic fields from 0 to 140 kOe from 30 to 80 K. A weak ferromagnetic signature seen below 10 kOe is due to the presence of about 2 wt % of $\text{Fe}_{1-x}\text{Ge}_x$.

system is in the frozen state whose boundaries overlap with the H_{c1} transition, therefore, the metamagnetic transition is only partially reversible. Above this point, the glass state is thermally removed, and the metamagnetic transition becomes fully reversible. In addition, similar field-induced magnetic transitions with strong hysteresis were also observed in Gd_5Ge_4 and $\text{Dy}_5\text{Si}_3\text{Ge}$ due to the first-order magnetostructural phase transitions.^{38,42} Therefore, the possibility of a magnetic-field-induced structural phase transition in DyFe_4Ge_2 cannot be ruled out. In addition, we notice that the magnetization is not saturated (it remains just about $7.2 \mu_B/\text{f.u.}$) (where f.u. represents formula unit) even at 140 kOe, indicating a possible ferrimagnetic (FIM) state at this field where Dy and Fe moments remain antiparallel.

Figure 8 shows the field dependence of the magnetization of DyFe_4Ge_2 , measured from 30 to 80 K. The magnetic-field-induced transitions are observed up to 50 K in the $M(H)$ data. The observed metamagnetic transitions are relatively smooth. The hysteresis at the first metamagnetic transition (H_{c1}) is gradually reduced as the temperature increases and finally disappears at ~ 40 K. For the second transition (H_{c2}), the hysteresis disappears between 10 and 20 K (see Fig. 7).

As a further characterization of the magnetic glasslike state in DyFe_4Ge_2 , the thermoremanent magnetization as a function of time, measured at 5 and 15 K, is shown in Fig. 9. For this measurement, the sample was as follows: (1) cooled from 300 K to the desired temperature in the zero field, (2) a magnetic field of 1000 Oe was applied for 1000 s, and (3) the field was switched off, and remanent magnetization was then recorded as a function of time. It is observed that the $M(t)$ decay is remarkably slow, and nonzero remanence exists after 6 h. The remanence and the long-time magnetic relaxation effects are the characteristic features of magnetic glasses. In addition, the time dependence of $M(t)$ fits to the logarithmic time dependence $M(t) = M_0(T) - S(T)\ln(t + t_0)$, typically observed in metallic spin glasses, was determined. The values for the two temperature-dependent fitting parameters are $M_0(T) = 0.583$ and 0.301 emu/g, $S(T) = 1.965 \times 10^{-3}$ and

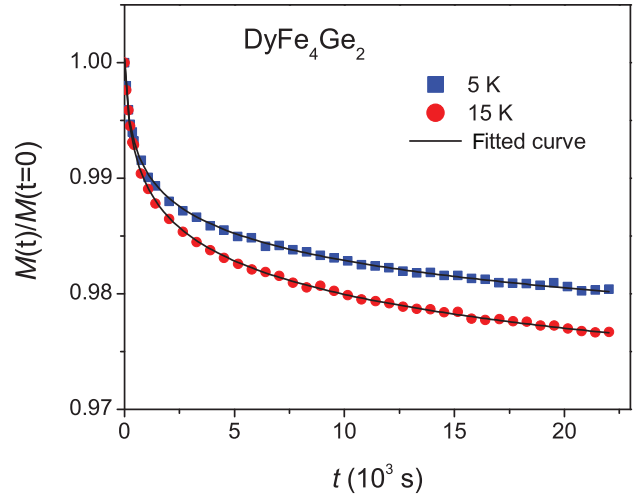


FIG. 9. (Color online) Isothermal remanent magnetization as a function of time measured at 5 and 15 K, respectively. The solid line represents the logarithmic fit of the decay.

1.255×10^{-3} emu/g, and $t_0 = 62$ and 84 s, for 5 and 15 K, respectively.

C. Heat capacity

The heat capacity of DyFe_4Ge_2 was measured on heating under different magnetic fields (0, 1, 10, 30, and 50 kOe) as shown in Fig. 10. Multiple magnetic phase transitions in the compound are clearly seen. In most cases, the anomalies in the heat capacity data coincide with the corresponding transitions seen in the magnetization data. However, no signature of a magnetic transition at $T_{f3} = 15$ K is found in the $C_p(T)$ curves. This too, is in agreement with the previous freezing point observations because this transition is generally not manifested as a distinct anomaly on the C_p plot.⁴³

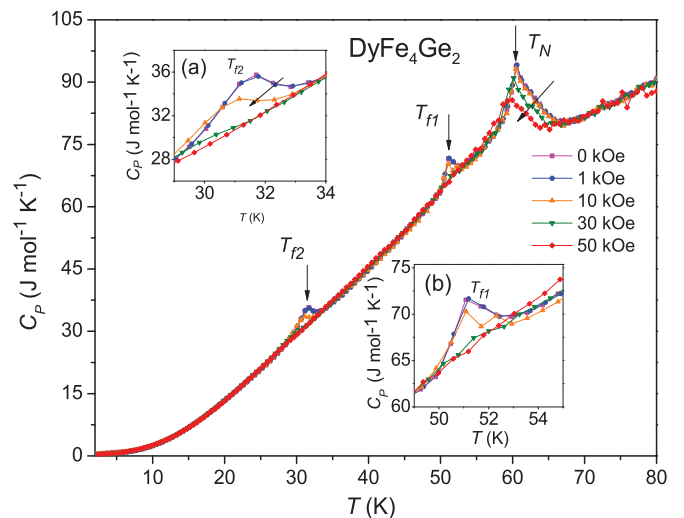


FIG. 10. (Color online) Temperature dependencies of the heat capacity (C_p) of DyFe_4Ge_2 measured in magnetic fields from 0 to 50 kOe. Insets (a) and (b) show the expanded view of the details of the regions around the first two transitions.

Furthermore, we note that the applied magnetic field strongly suppresses the anomalies both at the T_{f1} and at the T_{f2} as shown in the insets of Fig. 10. A small kink at T_{f2} shifts to a lower temperature in 10 kOe and then disappears for $H = 30$ kOe. For the transition at T_{f1} , the peak almost does not change below the 10 kOe field, but it also disappears when the field is greater than 30 kOe. The heat capacity peak at T_N becomes progressively less sharp, broadened, and shifts towards the lower temperature as shown in Fig. 10 by the arrow, confirming the antiferromagnetic ordering at this transition.

Our results show that the antiferromagnetic ordering temperature is 62 K, which is higher than the value observed by neutron diffraction [55 K (Ref. 20)]. In addition, other two transitions T_{f1} and T_{f2} , observed at 45 and 28 K, in both the low-temperature XRD and the neutron diffraction were claimed to be of first-order nature. Based on our findings, the phase transition at $T_{f2} = 32$ K is, indeed, of first-order nature as the magnetization curves between FCC and FCW clearly exhibit thermomagnetic irreversibility. However, the transition at T_{f1} (52 K, corresponding to the transition at 45 K in the neutron diffraction result) cannot be classified with certainty as first order because no thermal hysteresis is observed. On the other hand, both $C_P(T)$ anomalies observed at T_{f1} and T_{f2} and their behavior with the magnetic field are very similar. The magnetocaloric effect estimated using both the $M(H)$ data and the heat capacity data is small ($\Delta S_M \leq -1.8 \text{ J kg}^{-1} \text{ K}^{-1}$) for all of the transitions, i.e., at T_{f1} , T_{f2} , and T_N .

D. XRD measurements

Temperature-dependent XRD measurements show that the antiferromagnetic transition at T_N is coupled with a structural transition from $P4_2/mnm$ to $Cmmm$, which agrees with the result of Schobinger-Papamantellos and co-workers.^{18,20} Figure 11 presents the temperature dependencies of lattice parameters and unit-cell volume of DyFe_4Ge_2 , measured during cooling of the sample in the zero field. The thermal strain along the a and c axes varies nearly linearly above 65 K, and the coefficients of thermal expansion are $\alpha_a = 9.79 \times 10^{-6} \text{ K}^{-1}$ and $\alpha_c = 1.51 \times 10^{-5} \text{ K}^{-1}$. Below ~ 60 K, the tetragonal lattice begins to distort into the orthorhombic one as seen by the difference between the a and the b unit-cell dimensions (the identical a and b unit-cell dimensions in the tetragonal are shown as $a\sqrt{2}$ in Fig. 11 to allow direct comparison): b decreases and a increases rapidly upon lowering the temperature. At the same time, no volume discontinuity has been observed (or, at least, the discontinuity is smaller than the sensitivity limit ~ 40 – 80 ppm of our experiment), and therefore, the transition at T_N is either second order or very weak first order, which is consistent with the absence of hysteresis in the magnetization data. We also note that the accuracy of our powder diffraction data is insufficient to detect volume discontinuity at T_{f2} , which is the first-order phase transition.

IV. THEORETICAL INVESTIGATIONS

In order to better understand the magnetism and structure of DyFe_4Ge_2 , we have performed first-principles electronic structure calculations using the local spin density approx-

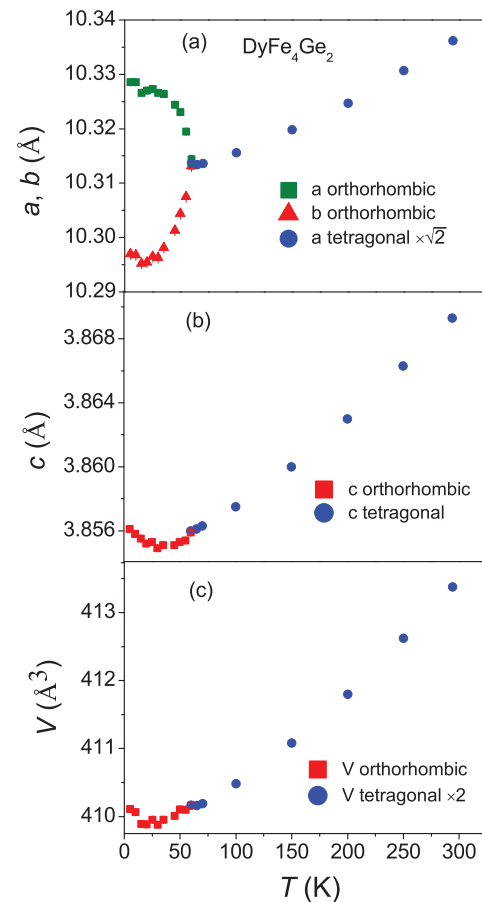


FIG. 11. (Color online) The variation in lattice parameters (a) a , b , (b) c , and (c) unit-cell volume V of DyFe_4Ge_2 with temperatures from 5 to 300 K.

imation (LSDA) including the Hubbard on-site parameter (LSDA + U) (Ref. 44) approach within the tight-binding linear muffin-tin orbital band structure method.^{45,46} Since the Coulomb repulsion between $4f$ electrons (U) and exchange interaction between localized $4f$ electrons (J) are not known for this system, we have employed $U = 6.7$ and $J = 0.7$ eV—well-known parameters for Gd atoms⁴⁴ in elemental gadolinium and Gd-based materials—also for Dy atoms as model parameters in DyFe_4Ge_2 . This approach has been successfully applied for rare-earth-based magnetic systems; we refer readers to some of our recent papers.^{47–56}

Our low-temperature XRD experimental results indicate that DyFe_4Ge_2 undergoes a transformation from the high-temperature PM tetragonal ($P4_2/mnm$) to the low-temperature AFM orthorhombic ($Cmmm$) structure at ~ 60 K. Here, we have performed two sets of the electronic structure calculations. The first set of calculations uses the tetragonal structure with atomic positions and lattice constants determined at 65 K, and the second set uses the orthorhombic structure with atomic positions and lattice constants determined at 10 K. These structural parameters are quite similar to those reported earlier in Ref. 18. It should be mentioned here that each independent atom [i.e., Dy ($2b$), Fe ($8i$), and Ge ($4g$)] splits into two nonequivalent atoms [i.e., Dy₁ ($2d$) and Dy₂ ($2b$), Fe₁ ($8p$) and Fe₂ ($8q$), and Ge₁ ($4g$) and Ge₂ ($4j$)] when the tetragonal DyFe_4Ge_2 transforms to the orthorhombic DyFe_4Ge_2 .

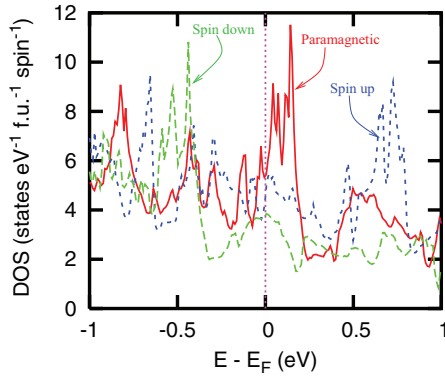


FIG. 12. (Color online) The paramagnetic and spin-polarized conduction electron (*spd*) density of states of DyFe_4Ge_2 in the tetragonal ($P4_2/mnm$) structure around the Fermi level.

Figure 12 shows the conduction electron (*spd*) density of states of DyFe_4Ge_2 around the Fermi level in the tetragonal ($P4_2/mnm$) structure. The paramagnetic density of states just above the Fermi level splits into spin up at ~ 0.75 eV and spin down at ~ -0.5 eV peaks in the spin-polarized calculations, indicating a large band splitting energy of ~ 1.25 eV. Here, the density of states peaks and the large band splitting are mainly contributed by Fe when the 3*d* states of Fe hybridize with the 5*d* states of Dy. Of course, the 5*d* electrons of the Dy spin are polarized due to the indirect 4*f*-4*f* exchange in DyFe_4Ge_2 . This Fe band splitting introduces an imbalance in the spin-up and spin-down density of states giving rise to a Fe 3*d* magnetic moment of $-1.35 \mu_B$. The Fe 3*d* moment is negative because the heavy lanthanide and transition metal spins align antiparallel to each other giving rise to spin-up Dy 5*d* and spin-down Fe 3*d* hybridizations. Since the *s* and *p* bands are quite broad compared to the 3*d* bands, the *s*- and *p*-band splitting is negligible, contributing nearly zero *s* and *p* moments.

Figure 13 shows 4*f* density of states of Dy in tetragonal DyFe_4Ge_2 . The spin-up density of states is split into five distinct bands and is located around -8 eV, and the unoccupied spin-down density of states is also split and is located around 2 eV. This splitting is due to the crystalline electric-field effect arising from the anisotropic 4*f* charge densities. The occupied spin-down density of states is centered at ~ -4.35 eV. The

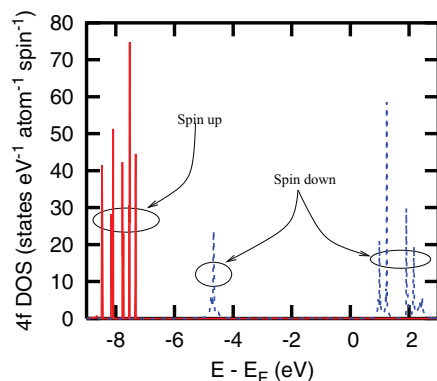


FIG. 13. (Color online) The 4*f* density of states of Dy in the tetragonal DyFe_4Ge_2 .

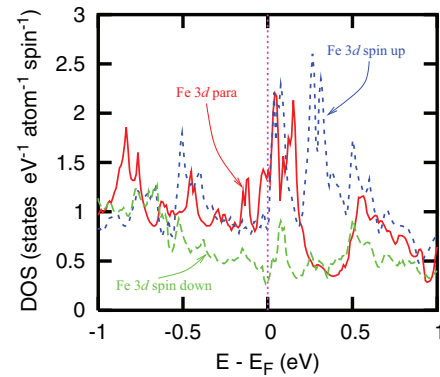


FIG. 14. (Color online) The paramagnetic and spin-polarized conduction electron (*spd*) density of states around the Fermi level of Fe in orthorhombic ($Cmmm$) DyFe_4Ge_2 .

difference between the integrated spin-up and spin-down 4*f* states up to the Fermi level gives rise to the 4*f* spin moment of $4.95 \mu_B$. It should be mentioned here that the orbital moment, contributed from the half-filled 4*f* orbitals, is $5 \mu_B$. Therefore, the total 4*f* moment of Dy is $9.95 \mu_B$ in the tetragonal ($P4_2/mnm$) DyFe_4Ge_2 . The indirect 4*f*-4*f* exchange, commonly known as the RKKY interaction, spin polarizes the conduction (mainly 5*d*) electrons, resulting in a 5*d* moment of Dy totaling $0.27 \mu_B$ in tetragonal DyFe_4Ge_2 . Since the *s* and *p* states are quite broad, the spin polarized *s* and *p* moments due to the indirect 4*f*-4*f* exchange are less than $0.05 \mu_B$.

Our temperature-dependent XRD results and the previous neutron diffraction experiments show that the low-temperature crystal structure of DyFe_4Ge_2 is orthorhombic. It orders antiferromagnetically below 62 K. The two sublattices Dy_1 and Dy_2 align antiparallel. Here, we have performed antiferromagnetic calculations with this alignment. In Fig. 14, we show the 3*d* density of the Fe in this structure, which is different from that of the Fe in the tetragonal structure (compare Figs. 12 and 14). Although the paramagnetic peak just above the Fermi level looks similar in both structures, the spin-up peak appears close to the DOS peak in the paramagnetic state. The spin-down peak at ~ -0.5 eV in the tetragonal structure is no longer present in the orthorhombic structure. These results indicate that the crystallographic change brings significant change in the local density of states of the transition metal component of this rare-earth-containing compound. The change in the crystal and magnetic structures, which brings change in the integrated spin-up and spin-down densities of states, gives rise to a $-1.14 \mu_B$ 3*d* moment for Fe, which is 16% smaller compared to the Fe moment in the tetragonal DyFe_4Ge_2 . The *s* and *p* moments remain negligible as in the tetragonal DyFe_4Ge_2 .

The 4*f* density of states of Dy in the antiferromagnetic orthorhombic DyFe_4Ge_2 (Fig. 15) and in ferrimagnetic tetragonal DyFe_4Ge_2 (Fig. 13) is quite similar. The only difference is that the unoccupied 4*f* states split into a greater number of states in the antiferromagnetic orthorhombic DyFe_4Ge_2 . Furthermore, the 4*f* spin moment of Dy in orthorhombic DyFe_4Ge_2 is $4.96 \mu_B$, which is identical to the Dy 4*f* spin moment in the tetragonal DyFe_4Ge_2 . This indicates that the 4*f* local moments in the two different crystal and magnetic structures are identical, which is not unusual because, in

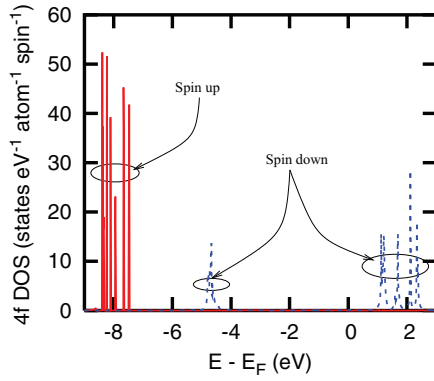


FIG. 15. (Color online) The 4*f* density of states of Dy in the antiferromagnetic orthorhombic DyFe₄Ge₂.

both tetragonal and orthorhombic crystal structures, the 4*f* moments are localized well below the Fermi level. But the spin polarized 5*d* moment in the Dy in the antiferromagnetic orthorhombic DyFe₄Ge₂ is 0.17 μ_B , which is 37% smaller than the 5*d* moments of Dy in the ferrimagnetic tetragonal DyFe₄Ge₂. This shows that, when DyFe₄Ge₂ transforms from ferrimagnetic tetragonal to the antiferromagnetic orthorhombic structure, the 5*d* spin polarization due to the indirect 4*f*-4*f* exchange is significantly reduced because of the rearrangement of the *spd* density of states around the Fermi level, which may be the reason for the magnetic state and crystal structure changes in this compound.

The paramagnetic total energy is lower by 101.8 meV/cell compared to the ferrimagnetic total energy in the tetragonal DyFe₄Ge₂, which indicates the stability of the paramagnetic tetragonal state in this structure. The tetragonal DyFe₄Ge₂ is, indeed, paramagnetic experimentally. On the other hand, the ferrimagnetic total energy is lower than the antiferromagnetic total energy in the orthorhombic structure of DyFe₄Ge₂. Experimentally, the ferrimagnetic state is the stable state with the application of the magnetic field, but the zero magnetic field state is antiferromagnetic. Since these total energy calculations are performed assuming collinear alignment of Dy spins without initially imposing the moments on Fe atoms, it is not surprising that the calculated magnetic ground state matches the state which is stable with the application of the magnetic field. Although, initially, we do not impose any moments on Fe, after self-consistent electronic structure calculations, the Fe moments become negative (coupling antiparallel to the Dy moments) in both ferrimagnetic tetragonal DyFe₄Ge₂ and orthorhombic ferrimagnetic or antiferromagnetic DyFe₄Ge₂. As pointed out earlier, these Fe moments are due to the hybridization of Fe 3*d* with Dy 5*d*, which are spin polarized by the indirect 4*f*-4*f* exchange.

V. PHASE DIAGRAM

Using the results of the ac and dc magnetic measurements, heat capacity of the bulk sample, and x-ray powder diffraction studies, the magnetic and structural phase diagram was constructed, see Fig. 16. The structure of the high-temperature paramagnetic phase is tetragonal. In the ordered state, four different (antiferromagnetic) regions can be distinguished as denoted by the frozen (FS), AFM I, AFM II, and AFM III states,

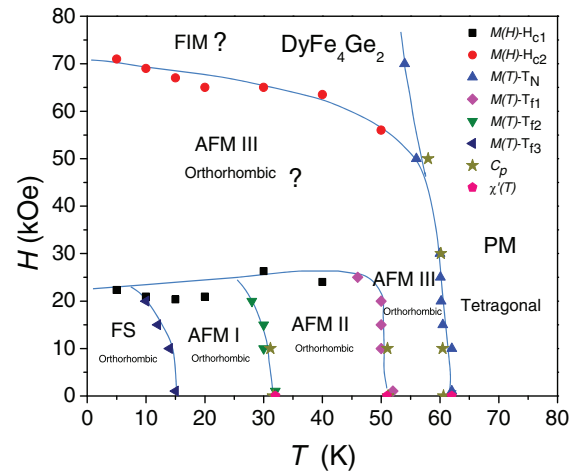


FIG. 16. (Color online) The temperature magnetic field phase diagram of DyFe₄Ge₂.

respectively, when the magnetic field is below H_{c1} . All of these states have orthorhombic crystal structures. The first critical field H_{c1} corresponds to the field-induced first-order magnetic transition from the frozen, AFM I, or AFM II phases to the AFM III phase. The crystal structure of AFM III is assumed to be orthorhombic based on the low magnetic field behaviors of the AFM III phase, but this needs to be verified. The second critical field H_{c2} indicates a second metamagnetic phase transition from the AFM III phase to the FIM state. At present, the crystal structure of the ferrimagnetic state is unknown.

VI. SUMMARY AND CONCLUSION

Detailed experimental investigations of the magnetization and heat capacity of DyFe₄Ge₂ indicate the existence of four magnetic phase transitions: the antiferromagnetic ordering at 62 K followed by three transitions at 52 (T_{f1}), 32 K (T_{f2}), and 15 K (T_{f3}). The transition at T_{f2} is marked by a strong thermal hysteresis in low field $M(T)$ measurements. The two low-temperature transitions (T_{f1}, T_{f2}) are due to spin reorientations of the Dy and Fe sublattices, and the high-temperature transition is an order-disorder one. The absence of the anomaly around freezing point T_{f3} in the temperature-dependent heat capacity and the very slow logarithmic decay of the remanence reveal a reentrant magnetic glassy state that exists at temperatures below T_{f3} . Two field-induced steplike metamagnetic phase transitions have been observed in $M(H)$ measurements between 2 and 50 K. They both exhibit field hysteresis, indicating their first-order nature; the exact nature of these transitions requires further investigation. The first-principles electronic structure calculations show that the indirect 4*f*-4*f* exchange spin polarizes 5*d* Dy, and the hybridization between spin-up Dy 5*d* and spin-down Fe 3*d* gives rise to antiparallel Dy and Fe moments in both tetragonal and orthorhombic structures of DyFe₄Ge₂. The paramagnetic tetragonal structure of DyFe₄Ge₂ is the stable structure in the paramagnetic state. The calculations with collinear Dy arrangements show ferrimagnetic orthorhombic DyFe₄Ge₂ as the ground-state structure.

ACKNOWLEDGMENTS

This work was supported by the US Department of Energy, Office of Basic Energy Science, Division of Materials Sciences

and Engineering. The research was performed at the Ames Laboratory operated for the US Department of Energy by Iowa State University under Contract No. DE-AC02-07CH11358.

*Corresponding author: liujing@iastate.edu

- ¹K. A. Gschneidner, Jr., V. K. Pecharsky, and A. O. Tsokol, *Rep. Prog. Phys.* **68**, 1479 (2005).
- ²L. Morellon, P. A. Algarabel, M. R. Ibarra, J. Blasco, B. Garcia-Landa, Z. Arnold, and F. Albertini, *Phys. Rev. B* **58**, R14721 (1998).
- ³E. M. Levin, V. K. Pecharsky, and K. A. Gschneidner, Jr., *Phys. Rev. B* **60**, 7993 (1999).
- ⁴V. K. Pecharsky and K. A. Gschneidner, Jr., *Phys. Rev. Lett.* **78**, 4494 (1997).
- ⁵V. K. Pecharsky and K. A. Gschneidner, Jr., *Appl. Phys. Lett.* **70**, 3299 (1997).
- ⁶V. K. Pecharsky and K. A. Gschneidner, Jr., *J. Magn. Magn. Mater.* **200**, 44 (1997).
- ⁷A. Giguère, M. Foldeaki, B. Ravi Gopal, R. Chahine, T. K. Bose, A. Frydman, and J. A. Barclay, *Phys. Rev. Lett.* **83**, 2262 (1999).
- ⁸K. A. Gschneidner, Jr., V. K. Pecharsky, E. Brück, H. G. M. Duijn, and E. M. Levin, *Phys. Rev. Lett.* **85**, 4190 (2000).
- ⁹W. Choe, V. K. Pecharsky, A. O. Pecharsky, K. A. Gschneidner, Jr., V. G. Young, Jr., and G. J. Miller, *Phys. Rev. Lett.* **84**, 4617 (2000).
- ¹⁰V. K. Pecharsky, A. P. Holm, K. A. Gschneidner, Jr., and R. Rink, *Phys. Rev. Lett.* **91**, 197204 (2003).
- ¹¹H. Wada and Y. Tanabe, *Appl. Phys. Lett.* **79**, 3302 (2001).
- ¹²O. Tegusa, E. Brück, L. Zhang, Dagula, K. H. J. Buschow, and F. R. de Boer, *Physica B* **319**, 174 (2002).
- ¹³J. B. A. Hamer, R. Daou, S. Özcan, N. D. Mathur, D. J. Fray, and K. G. Sandeman, *J. Magn. Magn. Mater.* **321**, 3535 (2009).
- ¹⁴S. Fujieda, A. Fujita, and K. Fukamichi, *Appl. Phys. Lett.* **81**, 1276 (2002).
- ¹⁵P. Schobinger-Papamantellos, J. Rodríguez-Carvajal, G. André, C. H. de Groot, F. R. de Boer, and K. H. J. Buschow, *J. Magn. Magn. Mater.* **191**, 261 (1999).
- ¹⁶P. Schobinger-Papamantellos, J. Rodríguez-Carvajal, G. André, N. P. Duong, K. H. J. Buschow, and P. Tolédano, *J. Magn. Magn. Mater.* **236**, 14 (2001).
- ¹⁷P. Schobinger-Papamantellos, J. Rodríguez-Carvajal, G. André, C. Ritter, and K. H. J. Buschow, *J. Magn. Magn. Mater.* **280**, 119 (2004).
- ¹⁸P. Schobinger-Papamantellos, J. Rodríguez-Carvajal, K. H. J. Buschow, E. Dooryhee, and A. N. Fitch, *J. Magn. Magn. Mater.* **300**, 315 (2006).
- ¹⁹P. Schobinger-Papamantellos, K. H. J. Buschow, and J. Rodríguez-Carvajal, *J. Magn. Magn. Mater.* **324**, 3709 (2012).
- ²⁰P. Schobinger-Papamantellos, J. Rodríguez-Carvajal, G. André, and K. H. J. Buschow, *J. Magn. Magn. Mater.* **300**, 333 (2006).
- ²¹O. Y. Oleksyn, Y. K. Gorelenko, and O. I. Bodak, Proceedings of the 10th International Conference on Solid Compounds of Transition Elements (unpublished).
- ²²A. M. Mulders, P. C. M. Gubbens, Q. A. Li, F. R. de Boer, and K. H. J. Buschow, *J. Alloys Compd.* **221**, 133 (1995).
- ²³P. Schobinger-Papamantellos, J. Rodríguez-Carvajal, and K. H. J. Buschow, *J. Magn. Magn. Mater.* **310**, 63 (2007).
- ²⁴P. Schobinger-Papamantellos, J. Rodríguez-Carvajal, G. André, K. H. J. Buschow, E. Dooryhee, and A. N. Fitch, *J. Magn. Magn. Mater.* **250**, 225 (2002).
- ²⁵P. C. M. Gubbens, B. D. van Dijk, A. M. Mulders, S. J. Harker, and K. H. J. Buschow, *J. Alloys Compd.* **319**, 1 (2001).
- ²⁶F. Canepa, S. Cirafici, F. Merlo, M. Pani, L. Carpaneto, and M. R. Cimberle, *J. Alloys Compd.* **266**, 26 (1998).
- ²⁷V. K. Pecharsky, J. O. Moorman, and K. A. Gschneidner, Jr., *Rev. Sci. Instrum.* **68**, 4196 (1997).
- ²⁸B. Hunter, RIETICA—A Visual Rietveld Program, International Union of Crystallography Commission on Powder Diffraction Newsletter, No. 20 (1998).
- ²⁹A. Szytula, S. Baran, J. Leciejewicz, B. Penc, N. Stüsser, Y. Ding, A. Zygunt, and J. Zukrowski, *J. Phys.: Condens. Matter* **9**, 6781 (1997).
- ³⁰P. A. Joy and S. K. Date, *J. Magn. Magn. Mater.* **218**, 229 (2000).
- ³¹K. Binder and A. P. Young, *Rev. Mod. Phys.* **58**, 801 (1986).
- ³²N. K. Singh, S. Agarwal, K. G. Suresh, R. Nirmala, A. K. Nigam, and S. K. Malik, *Phys. Rev. B* **72**, 014452 (2005).
- ³³J. L. Wang, C. Marquina, M. R. Ibarra, and G. H. Wu, *Phys. Rev. B* **73**, 094436 (2006).
- ³⁴S. B. Roy, A. K. Pradhan, P. Chaddah, and E. V. Sampathkumaran, *J. Phys.: Condens. Matter* **9**, 2465 (1997).
- ³⁵A. Tanaka, T. Tsutaoka, and T. Shigeoka, *Physica B* **403**, 3248 (2008).
- ³⁶R. Nirmala, Y. Mudryk, V. K. Pecharsky, and K. A. Gschneidner, Jr., *Phys. Rev. B* **76**, 014407 (2007).
- ³⁷N. K. Singh, K. G. Suresh, R. Nirmala, A. K. Nigam, and S. K. Malik, *J. Appl. Phys.* **101**, 093904 (2007).
- ³⁸Z. W. Ouyang, V. K. Pecharsky, K. A. Gschneidner, Jr., D. L. Schlagel, and T. A. Lograsso, *Phys. Rev. B* **74**, 024401 (2006).
- ³⁹M. K. Chattopadhyay, M. A. Manekar, A. O. Pecharsky, V. K. Pecharsky, K. A. Gschneidner, Jr., J. Moore, G. K. Perkins, Y. V. Bugoslavsky, S. B. Roy, P. Chaddah, and L. F. Cohen, *Phys. Rev. B* **70**, 214421 (2004).
- ⁴⁰S. B. Roy, M. K. Chattopadhyay, P. Chaddah, J. D. Moore, G. K. Perkins, L. F. Cohen, K. A. Gschneidner, Jr., and V. K. Pecharsky, *Phys. Rev. B* **74**, 012403 (2006).
- ⁴¹V. K. Pecharsky and K. A. Gschneidner, Jr., *Pure Appl. Chem.* **79**, 1383 (2007).
- ⁴²R. Nirmala, Y. Mudryk, V. K. Pecharsky, and K. A. Gschneidner, Jr., *Phys. Rev. B* **76**, 104417 (2007).
- ⁴³H. Tang, V. K. Pecharsky, K. A. Gschneidner, Jr., and A. O. Pecharsky, *Phys. Rev. B* **69**, 064410 (2004).
- ⁴⁴V. I. Anisimov, F. Aryasetiawan, and A. I. Lichtenstein, *J. Phys.: Condens. Matter* **9**, 767 (1997).
- ⁴⁵O. K. Andersen and O. Jepsen, *Phys. Rev. Lett.* **53**, 2571 (1984).
- ⁴⁶O. K. Andersen, *Phys. Rev. B* **12**, 3060 (1975).

- ⁴⁷D. Paudyal, Y. Mudryk, V. K. Pecharsky, and K. A. Gschneidner, Jr., *Phys. Rev. B* **84**, 014421 (2011).
- ⁴⁸M. Khan, D. Paudyal, Y. Mudryk, K. A. Gschneidner, Jr., and V. K. Pecharsky, *Phys. Rev. B* **83**, 134437 (2011).
- ⁴⁹D. Paudyal, Y. Mudryk, V. K. Pecharsky, and K. A. Gschneidner, Jr., *Phys. Rev. B* **82**, 144413 (2010).
- ⁵⁰Y. Mudryk, D. Paudyal, V. K. Pecharsky, K. A. Gschneidner, Jr., S. Misra, and G. J. Miller, *Phys. Rev. Lett.* **105**, 066401 (2010).
- ⁵¹N. K. Singh, D. Paudyal, Y. Mudryk, V. K. Pecharsky, and K. A. Gschneidner, Jr., *Phys. Rev. B* **79**, 094115 (2009).
- ⁵²D. Paudyal, Y. Mudryk, Y. B. Lee, V. K. Pecharsky, K. A. Gschneidner, Jr., and B. N. Harmon, *Phys. Rev. B* **78**, 184436 (2008).
- ⁵³D. Paudyal, V. K. Pecharsky, and K. A. Gschneidner, Jr., *J. Phys.: Condens. Matter* **20**, 235235 (2008).
- ⁵⁴Y. Mudryk, D. Paudyal, V. K. Pecharsky, and K. A. Gschneidner, Jr., *Phys. Rev. B* **77**, 024408 (2008).
- ⁵⁵D. Paudyal, V. K. Pecharsky, K. A. Gschneidner, Jr., and B. N. Harmon, *Phys. Rev. B* **75**, 094427 (2007).
- ⁵⁶D. Paudyal, V. K. Pecharsky, K. A. Gschneidner, Jr., and B. N. Harmon, *Phys. Rev. B* **73**, 144406 (2006).